Modeling the Tensile Strain Hardening Behavior of a Metastable AISI 301LN Austenitic Stainless Steel Pre-strained in Compression

Tulani W. Mukarati*, Roelf J. Mostert, Charles W. Siyasiya & Waldo E. Stumpf

Department of Materials Science and Metallurgical Engineering, University of Pretoria, Mineral Sciences Building, Lynnwood Rd and Roper St Hatfield, Pretoria, 0028, Republic of South Africa

*Correspondence to Tulani W. Mukarati. Email: u16378025@tuks.co.za.

Abstract

Boltzmann-type sigmoidal equations to model the tensile strain hardening and flow stress behavior of a metastable AISI 301LN austenitic stainless steel subjected to prior cold deformation have been developed. This model can be used in the numerical simulation of the energy absorbed by structures fabricated using this steel during collision events. In addition, it can also be used to establish the maximum allowable prior compressive strain through cold rolling which will result in a steel capable of adequate energy absorption. It was found that the compressive pre-strain had a strong effect on increasing the initial martensite content, increasing the tensile yield strength but reducing the ability of the material to absorb energy during subsequent tensile straining. In order to produce AISI 301LN crash-relevant structures for a vehicle, a cold rolling thickness reduction in the order of 20 pct or lower must be employed. This will result in the mechanical energy absorbed by the material of at least 210 MJ/m^3 in the event of a collision. The tensile strain hardening curves established for the pre-strained steel confirmed a high-strength coefficient value in the range of 1770 to 1790 MPa for the AISI 301LN steel at 30 °C. Neutron diffraction work, coupled with Electron backscatter diffraction (EBSD) analyses, studied the $\gamma \rightarrow \alpha'$ and ε martensitic transformation during compressive pre-straining, in order to explain the subsequent tensile strain hardening effects observed.

1 Introduction

Metastable austenitic steels hold great promise for use in structures where high energy absorption in the case of collisions is required, for the development of the so-called “crash-resistant” high-strength steels. The austenite-to-martensite transformation induced by plastic deformation is known to give rise to high work-hardening and energy adsorption rates.[1] Furthermore, these steels can be pre-strengthened by temper rolling so that the martensite constituent induced by compressive straining contributes to the increase in the yield strength, resulting in high yield strength values for the as-built structures. The development of constitutive equations describing the tensile strain hardening as a function of the prior compressive deformation, during temper rolling, specifically during subsequent tensile straining as one would encounter in a collision, is however challenging.

The work-hardening behavior of many engineering materials have been sufficiently described by the Hollomon’s power law,[2] which, however, provides some challenges at flow stresses close to the yield strength.

$$\sigma = K\varepsilon^n. \tag{1}$$

To overcome such challenges, this equation was modified by Swift for materials which show similar yield strengths but with varying strain hardening behavior by proposing an additional strain term, ε_o.[3]

$$\sigma = K(\varepsilon_o + \varepsilon)^n. \tag{2}$$

Pre-straining of metastable austenitic stainless steels by a process such as cold rolling results in high variability of yield strength values during subsequent tensile loading.[4] A modified Swift model has been proposed to account for the effect of compressive pre-strain on the flow properties during subsequent tensile reloading. This model was shown to be accurate for materials where the phase composition remains constant upon deformation, such as with low carbon steels.[5,6] For metastable austenitic steels such as AISI 301 LN, prior cold rolling stimulates the martensite transformation and instills high levels of yield strength. It is, however, unlikely that the modified Swift models will be successful in describing the subsequent flow behavior during tensile reloading, due to the complex effects that the martensite formation has on the flow behavior. Not only the additional strain term is needed but additional stress factor as well due to varying yield strength because of pre-existing martensite which has been induced during prior cold rolling.

The Ludwik modification of the Hollomon equation added an additional stress factor (σ_o) for materials which show varying yield strength values with similar strain hardening behavior.[3]

$$\sigma = \sigma_o + K\varepsilon^n. \tag{3}$$

The Ludwik equation was, however, found to be unable to model the flow behavior of AISI 301LN steel, and it is therefore unlikely to be successful in accounting for the effect of cold rolling pre-strain.[3] Earlier work by the current authors demonstrated that a Boltzmann sigmoidal strain hardening equation was successful in the calculation of the tensile flow behavior of this steel over a wide range of temperatures.[7]

$$\log \sigma = A + (B - A)\left[1 + \exp(\log \varepsilon - \alpha_s)(\beta_s)^{-1}\right]^{-1}, \tag{4}$$

where σ is the true stress in MPa, A is the maximum log of true stress ($\log \sigma_{max}$) when the sigmoidal function levels off after the martensitic transformation reaches saturation point, B is the minimum log of true stress ($\log \sigma_{min}$) at the beginning of the sigmoidal curve before any significant martensitic transformation in tension, ε is the true strain, α_s is the maximum strain sensitivity which corresponds to the log true strain value where there is a maximum slope of the log–log plot of the true stress–true strain curve, and β_s is a "Hill factor" derived from the sigmoidal nature of the log–log plots of the true stress–strain curves. The variable describes the steepness of the sigmoidal curve. The numerical value is given by, $\beta = (A - B)(4 \times n_{ipeak})^{-1}$, where n_{ipeak} is the peak instantaneous strain hardening exponent, which is the maximum instantaneous derivative of the sigmoidal function.

In the earlier work,[7] the effect of compressive pre-strain was, however, not analyzed. This paper therefore seeks to investigate the Boltzmann sigmoidal strain hardening function as a possible basis for modeling the tensile flow behavior of metastable austenitic steels following

compressive pre-straining through cold rolling at a temperature where a second phase transformation in 18-8 metastable austenitic steels occurs, with specific reference to AISI 301LN. The same mathematical form of equation seems to be able to quantitatively describe the variation of austenite-to-martensite transformation as a function of true strain.[9] This is due to the close relationship between strain hardening and strain-induced martensitic transformation (SIMT). The equations which have been reported in literature to model the behavior of the $\gamma \rightarrow \alpha'$ transformation as function of applied strain include the Olson and Cohen model,[8] the extended JMAK equation by Shin,[9] the Guimaraes model,[10] the Matsumura equation,[11,12] and the Gompertz model by Ahmedabadi,[13] Tavares,[14] and Naghizadeh[15] have not been tested on modeling the strain hardening behavior of metastable austenitic stainless steels. These works referenced have not produced equations which could be used for both martensite transformation and strain hardening.

A second aim of the work is to investigate the maximum prior cold deformation that can be applied, while still maintaining good tensile energy absorption during a collision event. It stands to reason that increased cold deformation will increase the initial martensite content and the yield strength, but it is likely that there will be a maximum yield strength gain which can be achieved before the tensile energy absorption capacity will be reduced to unacceptable levels.

2 Experimental Procedure

Cold rolling was done on an industrially produced AISI 301LN stainless steel sheet in annealed and pickled condition (as-received) to different gauges from 5 to 70 pct at room temperature with an interpass cooling in water at 25 °C. The plastic flow behavior of pre-strained material in compression was then studied by means of uniaxial tensile testing with interrupted tests that were done at 30 °C using a hydraulic universal tensile machine by Instron (1175 model) equipped with a 100 kN load cell fitted with an environmental chamber (3110 model) at an initial low strain rate of 6.67×10^{-4} s^{-1}. This strain rate was chosen to minimize adiabatic heating which results from high strain rates. A 50-mm-gauge contact extensometer (model 2630-112 by Instron) was used to determine the elongation of the samples upon deformation and was not removed until fracture. The experimental scatter of experimental values was included in all graphs and to some degree could have been caused by interruption during tensile deformation. Single experiments were performed. Tensile samples were machined according to ASTM E-8M standard.

The prior cold rolling had resulted in the formation of various amounts of martensitic phase depending on the degree of prior cold rolling as evaluated by means of Ferritescope instrument (Helmut Fisher GmbH, model MP3B). During tensile deformation, an indication of the percentage of strain-induced α'-martensite of all the specimens was again initially determined using the same Ferritescope instrument at 5 pct engineering strain intervals. The operational principle of the Ferritescope is based on the measurement of the magnetic permeability of the material. Ferritescope readings have been designed to quantify the fraction of delta ferrite (magnetic) in austenitic stainless-steel weld metal and need to be corrected if it is used to quantify martensite fractions. Ferritescope measurements were used as a quick and non-destructive approach for in-situ measurements of magnetic strain-induced α'-martensite content. The results of the Ferritescope readings were adjusted to true values of percentage α'-martensite by the established calibration curves using a combination of Vibrating Sample Magnetization (VSM) measurements, X-ray, and neutron diffraction analyses. A calibration factor of 1.62 (derived using compressive deformation),[16] and a calibration factor of 1.70

(derived using tensile deformation),[17] were found to be accurate to convert Ferritescope measurements to actual percentage of martensite content. A calibration factor of 1.70 (derived using tensile deformation) was found to be in good agreement with what was reported in the literature[18,19] and was used to convert Ferritescope measurements to arrive at the true α'-martensite content during interrupted tensile testing. Accurate determination of the volume fractions of the phase transformation upon progression of cold deformation of austenite is essential to have a good knowledge of the process. There was no need for thickness correction for Ferritescope measurements as the thickness of the samples were all greater than 2 mm.

In all cases during Ferritescope measurements, at least seven readings were taken on the surface of individual cold-rolled samples and tensile-deformed samples at different points within the uniform elongation region of the gauge length. The mean and standard deviations were calculated. The Ferritescope readings were taken under unloaded (unstressed) conditions when atoms are in their equilibrium positions to give a true magnetic response of the material. The Ferritescope device was calibrated using the standard δ-ferrite samples supplied with it. The samples for EBSD microstructural analysis were lightly ground and electropolished using a Struers Lectropol-5 equipment and A3 electrolyte at an operating voltage of 35 V at room temperature for 50 seconds. Samples for neutron diffraction analysis were machined using wire-cut electrical discharge machining and no further sample preparation was done to avoid further formation of strain-induced martensite during the process. Neutrons have much greater penetration depth as compared to scanning near the surface only as in EBSD microstructural analysis and X-ray diffraction analysis, hence the neutron diffraction technique analyzes a considerable larger volume as compared to the EBSD and XRD techniques. For chemical composition, see Table I and this is the same material as was studied in the previous works.[2,7,20]

Table I. Chemical Composition of Annealed and Pickled AISI 301LN as Supplied (Wt Pct)

C	Mn	P	S	Si	Cr	Ni	N	Cu	Mo	Fe
0.02	1.54	0.026	0.003	0.42	17.49	6.6	0.1133	0.15	0.16	balance

The initial percentage of austenite at 25 °C was determined as being 100 pct, using microscopical, diffraction analyses (X-ray and neutron) and magnetic methods.[21] The percentage of austenite (γ), α'- and ε-martensites of the selected samples were determined using X-ray and neutron diffraction analyses. The initial thickness of the steel sheets was 4.05 mm. The percentage of cold rolling was converted to true compressive strain by using the normal relationship between the thickness reduction, r and true strain, ε.

3 Results

The percentage of both α' and ε martensitic transformed, as a function of the percentage of prior cold rolling, is given in Figure 1. The volume fractions of ε-martensite were obtained solely using neutron diffraction analyses while volume fractions of α' martensite were obtained using adjusted Ferritescope readings. The neutron diffraction spectra for selected samples after different levels of prior cold rolling are as shown in Figure 2. The Ferritescope readings were multiplied by a calibration factor of 1.62 to convert to true values of percentage α'-martensite as was established using neutron diffraction analyses.[21] It was found that the ε-martensite increases to a maximum at relatively low levels of deformation, around $r \sim 0.15$ and then decreases to zero indicating, ε-martensite as an intermediate phase in the $\gamma \rightarrow \alpha'$ transformation. In the later stages of deformation ($r > 0.45$), no ε-martensite was detected indicating $\varepsilon \rightarrow \alpha'$

transformation at high compressive strains and it appears that further martensitic formation occurs in a direct $\gamma \rightarrow \alpha'$ transformation without any intermediate ε-martensite formation.

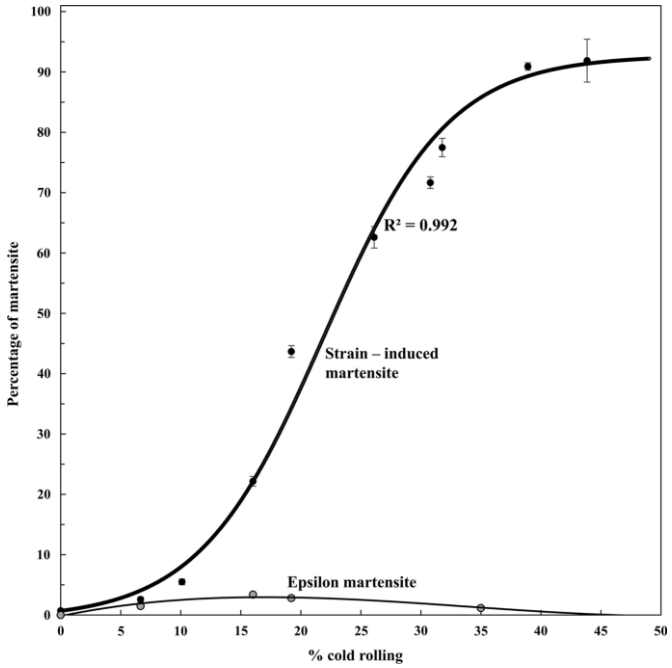

Fig. 1. The variation of percentage of both α' and ε martensite induced as a function of percentage of cold rolling at room temperature, with balance being austenite (γ)

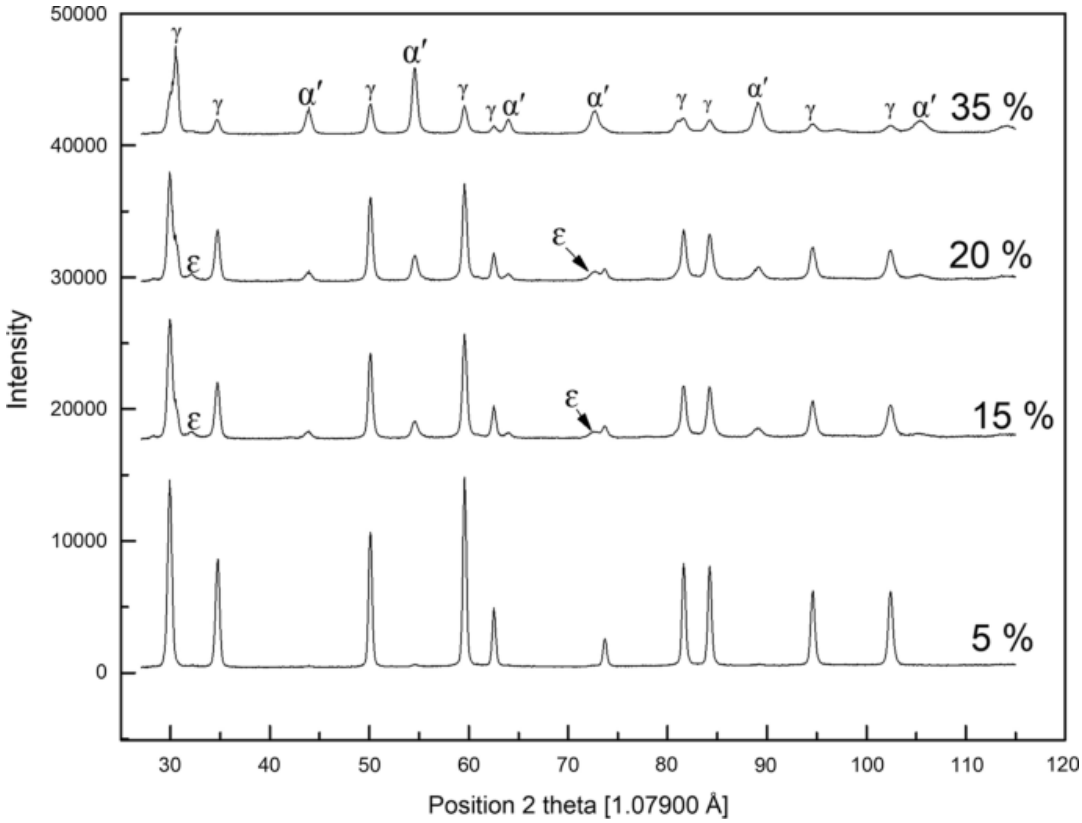

Fig. 2. Neutron diffraction patterns of deformed AISI 301LN metastable austenitic stainless steel

The as-received (annealed) microstructure was fully austenitic. EBSD microscopy was used to confirm the influence of cold rolling on the transformation of austenite to α'- and ε-martensite. Smaller amounts of ε-martensite after 10 pct cold rolling were visibly observed using EBSD as shown in Figure 3(a), whereas at higher deformations (30 pct cold rolling), no ε-martensite could be easily observed through EBSD as shown in Figure 3(b). The microstructural analysis using EBSD showed the morphology and distribution of phases and was not used for any phase quantification. This is because the EBSD technique provides inaccurate phase quantification due to the high density of dislocations formed during cold working. High density of dislocations leads to degraded backscatter Kikuchi diffraction patterns and high orientation gradients.

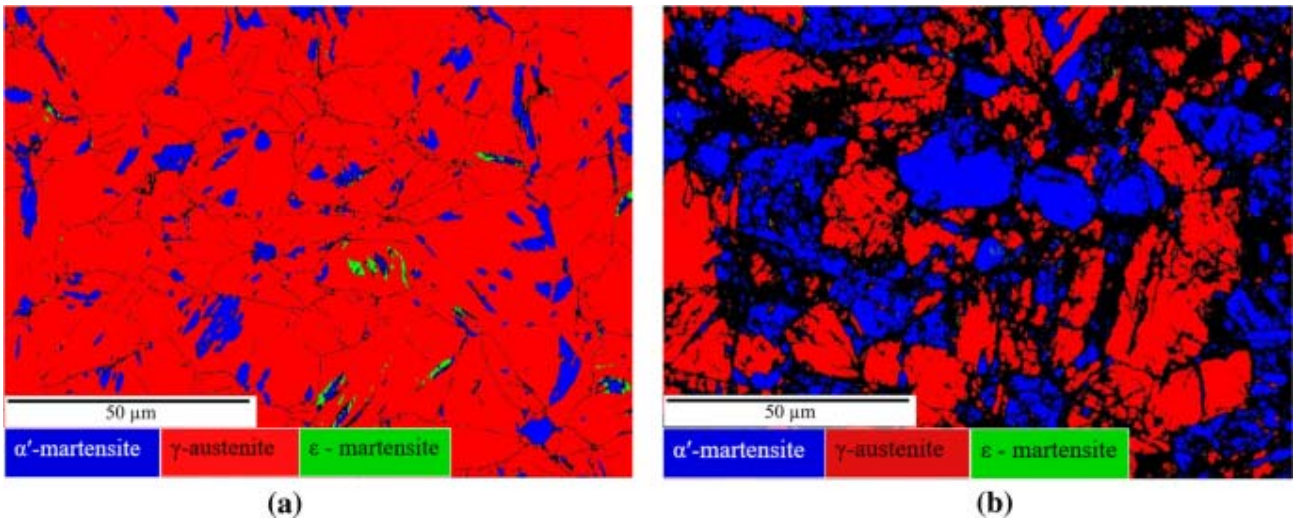

Fig. 3. EBSD images of AISI 301LN taken from the surface after (*a*) 10 pct cold rolling, (*b*) 32 pct cold rolling

The percentage of α'-martensite induced as a function of strain during tensile deformation after various degrees of prior cold rolling at 30 °C is shown in Figure 4. For no prior cold rolling and small percentages of prior cold rolling (5 pct), a fully sigmoidal relationship was observed between the percentage of martensite and the applied tensile strain. After higher degrees of prior cold rolling, the sigmoidal behavior was, however, largely lost.

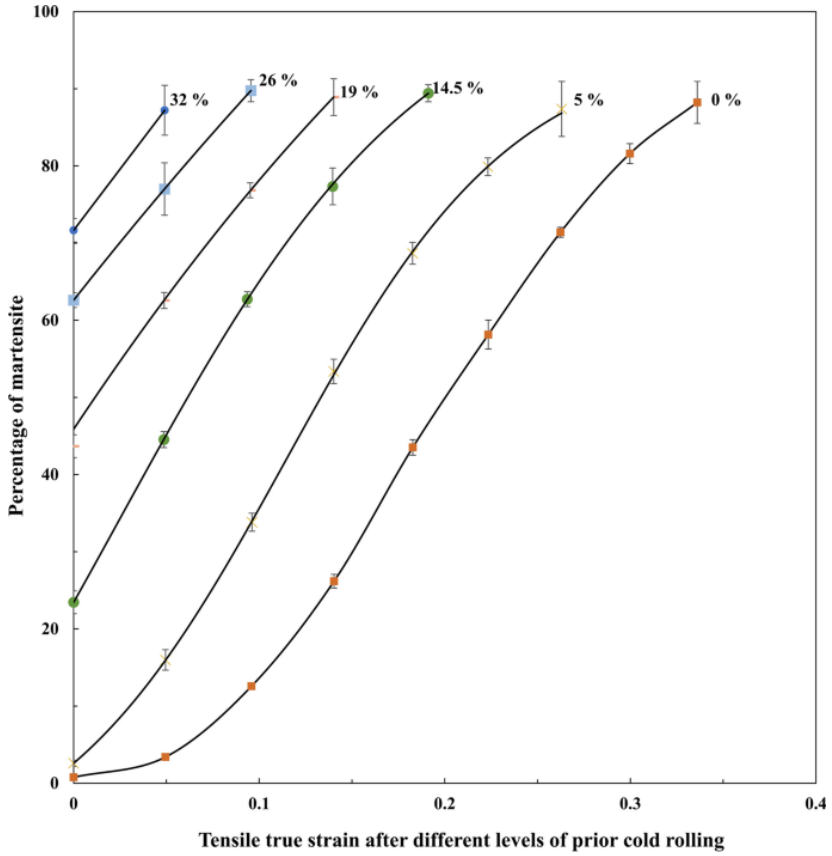

Fig. 4. Percentage of α'-martensite induced as a function of applied tensile strain after various degrees of prior cold rolling at 30 °C tested at an initial strain rate of 6.67×10^{-4} s^{-1}

Figure 5 shows the true stress–strain curves in tension after various degrees of prior cold rolling at room temperature, (25 °C). Plastic deformation decreases as the degree of prior cold rolling increases. The sample with no prior cold rolling exhibits yield point elongation plateau which disappears on samples which had received a higher amount of prior cold rolling. All true stress–strain curves indicate a transition from sigmoidal nature after low levels of prior cold rolling to non-sigmoidal nature after high levels of cold rolling.

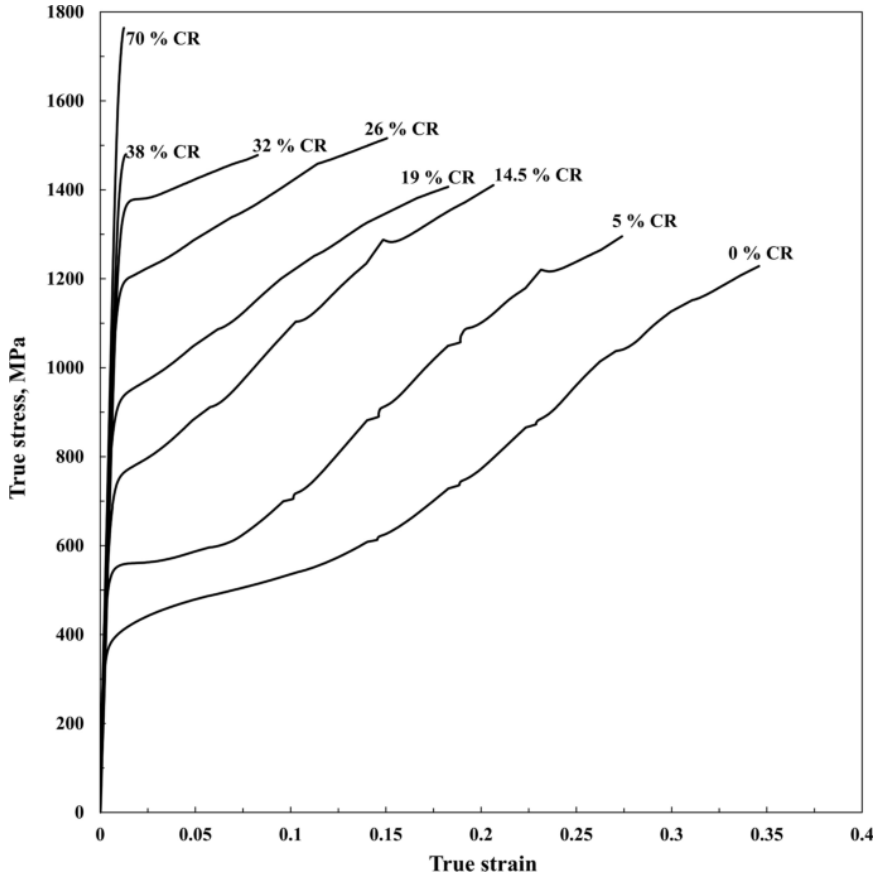

Fig. 5. True stress–strain curves of prior cold-rolled samples. Tensile testing performed at room temperature, (25 °C)

The different degrees of prior cold rolling had resulted in various volume fractions of strain-induced α'-martensite, as determined by the Ferritescope measurements corrected using a calibration curve established for compressive loading.[21] This resulted in a significant increase in the yield strength and tensile strength upon subsequent tensile deformation. The magnitude of the strength increase was strongly dependent on the percentage of prior cold rolling. The tensile strain hardening sigmoidal curves as a function of percentage of applied tensile strain is shown in Figure 6, obtained by a log–log plot of true stress–strain of the experimental tensile data, for true strain values corresponding to plastic deformation.

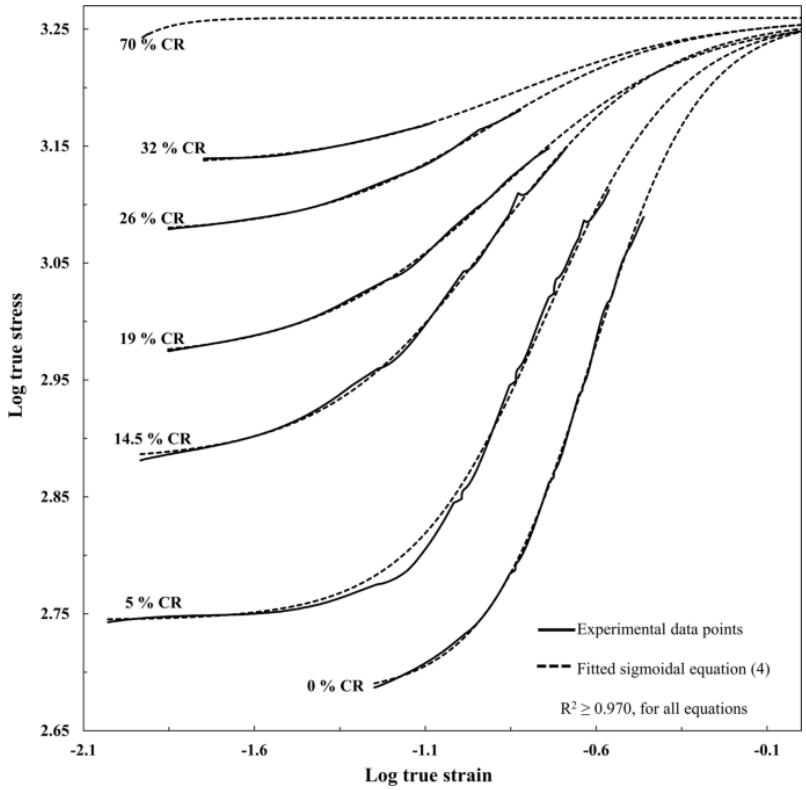

Fig. 6. The log–log plot of the tensile true stress–strain curves at 30 °C, after various levels of prior cold rolling showing sigmoidal flow stress behavior

The strain hardening response as a function of applied strain, at most levels of prior cold rolling shown in Figure 6, follows the same mathematical form (modified Boltzmann sigmoidal equation), Eq. [4], as was the case for the annealed material established earlier.[7] The mathematical sigmoidal Eq. [4] evaluated has three parameters that determine the strain hardening behavior: A, the maximum log of true stress ($\log \sigma_{max}$) in Figure 6 when the sigmoidal function levels off after the martensitic transformation reaches the saturation point; B as the minimum log of true stress ($\log \sigma_{min}$) at the beginning of the sigmoidal curve, before any significant martensitic transformation in tension; and α_s as the maximum strain sensitivity which corresponds to the log true strain value where there is a maximum slope of the log–log plot of the true stress–true strain curve (log of ε corresponding with peak slope of Figure 7).

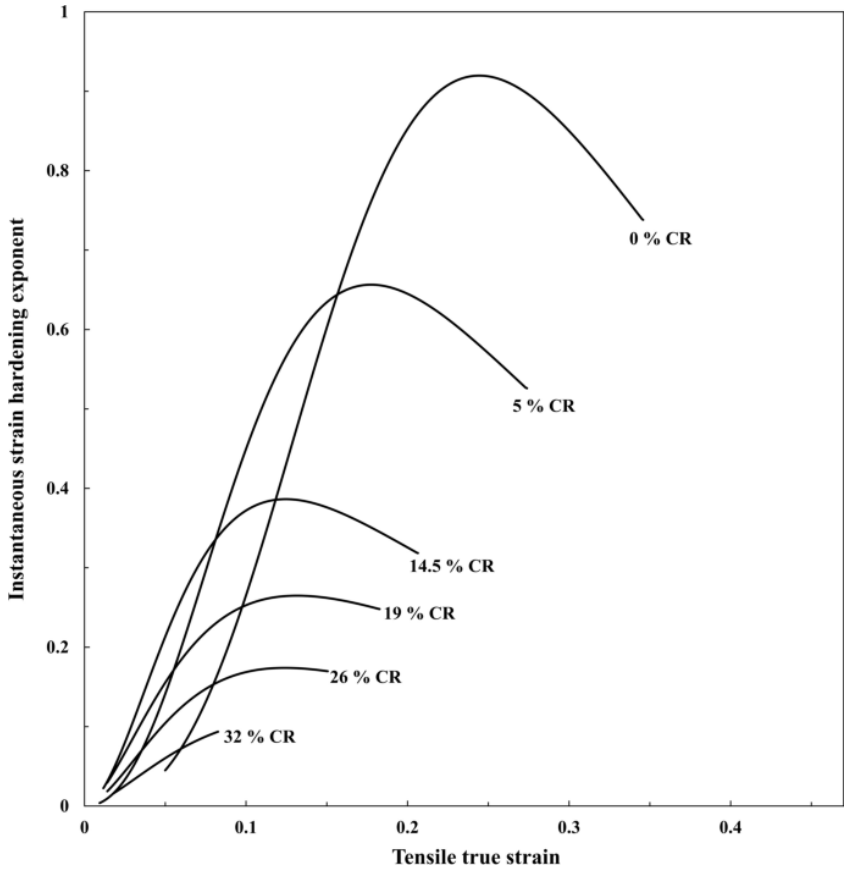

Fig. 7. Variation of tensile instantaneous strain hardening exponent, n_i as a function of prior thickness reduction and applied tensile strain at room temperature

Fitted sigmoidal curves through the experimental data were extended up to the true strain levels of 1.0, to arrive at estimates of the strength coefficient, K, which was found to be in the range of 1770 to 1790 MPa, as calculated from the convergence of sigmoidal hardening curves at log stress of ~ 3.25 (at log true strain of 0). The tensile testing was done with interruption at every 5 pct engineering strain to allow Ferritescope measurements to be taken as well as to prevent the adiabatic heating so that the deformation temperature remained close to 30 °C. Small portions of the data which correspond to unloading (removal of stress) and loading to the new yield point were removed on each interruption cycle during tensile deformation to develop a smooth curve in order to derive a continuous constitutive equation. The range of strength coefficients determined in this fashion was found to be in good agreement with the true tensile strength of approximately ~ 1715 MPa, determined after cold rolling to 63.2 pct (which is equivalent to the compressive true strain of 1 ≡ log true strain of 0) and tensile testing thereafter.

The instantaneous strain hardening exponent, (n_i)-values as defined by Dini *et al.*[22] and Soares *et al.*[23] were calculated as the instantaneous derivative of the log–log plot of Eq. [4], which was used to describe the mathematical relationship of the data shown in Figure 6. Figure 7 shows the variation of the instantaneous strain hardening exponent, n_i determined in tension as a function of true tensile strain (in the sigmoidal behavior region, shown in Figure 6) after various levels of prior cold rolling. The instantaneous strain hardening exponent (n_i)-values rapidly increase up to a peak n_i-value as a function of tensile strain and decreases sharply thereafter with further increase in applied tensile strain as shown in Figure 7, in a fashion

similar to that of the rate of $\gamma \rightarrow \alpha'$ strain-induced martensitic transformation per unit strain ($dV\alpha'/d\varepsilon$) which was observed by Mukarati *et al.*[21] for the same experimental conditions in the absence of prior cold rolling. The peak values in Figure 7 were, however, strongly dependent on the degree of prior cold rolling, showing a strong inverse trend.

Figure 8 shows the variation of peak instantaneous strain hardening exponent, n_{ipeak}-values as a function of initial amount of strain-induced α'-martensite formed during prior cold rolling and taken from Figure 7, showing a rapid decrease in the peak strain hardening response as the initial amount of martensite increases (due to increase in prior compressive strain). This behavior suggests that the tensile strain hardening of the austenite/martensite microstructure rapidly decreases with an increase in the percentage of martensite initially present.

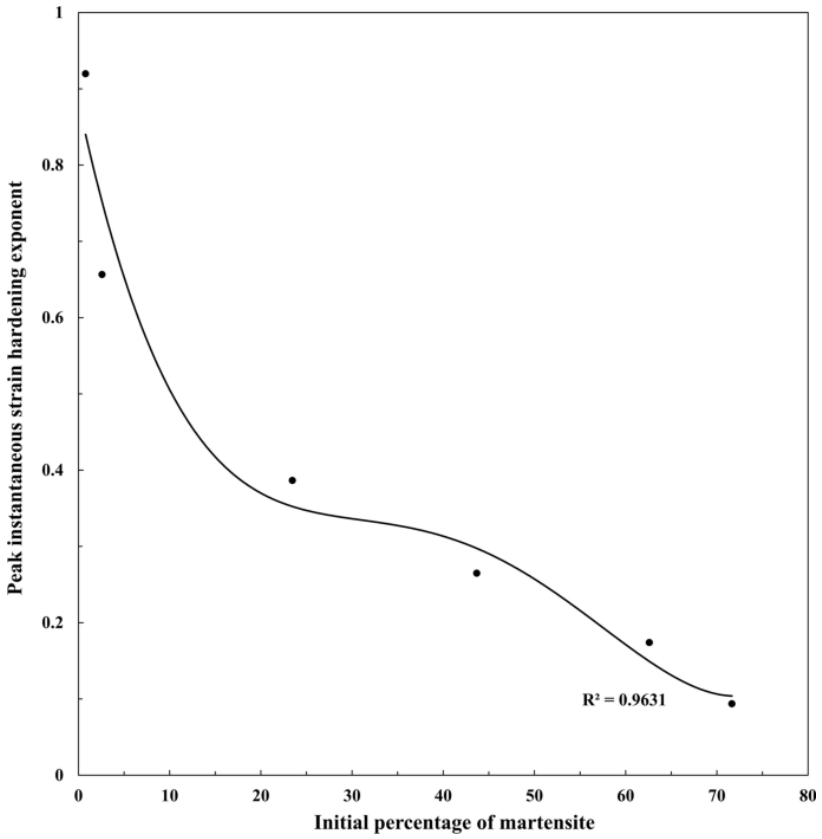

Fig. 8. Peak instantaneous tensile strain hardening exponent, n_{ipeak}, as a function of the initial percentage of α'-martensite induced during prior cold rolling

High tensile strain hardening was observed when high fractions of austenite were initially present and high strain hardening was associated with high tensile ductility (refer to Figure 6; 0 to 5 pct CR). The fraction of martensite phase present after cold rolling is critical for strength but it must be controlled within a stringent range as it has an adverse impact on tensile strain hardening and ductility.[21] The higher the volume fraction of strain-induced martensite present after cold rolling, the lower the volume fraction of austenite present, and the lower the subsequent strain hardening response in tension of the material will be. This behaviour is shown by the lower peak values of instantaneous strain hardening exponent, n_{ipeak} in Figure 8. Conversely, the material with a higher initial amount of austenite (low percentage of prior cold rolling and low amount of initial strain-induced martensite) exhibited higher peak values of

instantaneous strain hardening exponent, n_{ipeak}, due to the better strain hardening response of austenite.

The developed sigmoidal Eq. [4] can be utilized to describe the tensile strain hardening behavior for materials which had undergone prior compressive straining through cold rolling with different initial amounts of martensite at a given temperature. The modification is similar to the modification applied in developing the Swift model which has an additional term, ε_o, which accounts for compressive pre-strain. However, unlike the case of the Swift model, prior cold rolling of this metastable austenitic material introduces a strong increase of the yield strength due to martensite formation, hence, the *B* term in the sigmoidal Eq. [4], also increases with the increase in pre-strain. Equation [5] shows the variation of the *B* term as a function of pre-strain by compression.

$$B = 1.21 * \varepsilon_o + 2.69 \tag{5}$$

Pre-strain by compression results in an increase of the yield strength, as shown in Figure 5. The values of the B term were determined from individual sigmoidal equations used in fitting the log–log plots of the tensile true stress–strain curves at 30 °C, after various amounts of prior cold rolling as shown in Figure 6. The variation of the B term as a function of compressive pre-strain was found to be linear as shown in Eq. [5].

The A term in the sigmoidal Eq. [4] which was the maximum log of true stress (log σ_{max}) when the sigmoidal function levels off after the martensitic transformation reaches the saturation point was approximated as 3.25 for all cases. It was found that the sigmoidal hardening curves would converge at a log stress value of ~ 3.25 if plastic instability did not cause necking and early fracture. The value of 3.25 corresponds to a log true strain value of 0, which corresponds to a strength coefficient, *K* of approximately ~ 1780 MPa after deformation at 30 °C.

The α_s term, maximum strain sensitivity, in the sigmoidal Eq. [4] is the log strain value where there is a maximum slope of the log–log plot of the true stress–true strain curve, that is, the log of the true tensile strain corresponding to the maximum instantaneous strain hardening exponent. The true strain for the maximum slope eventually becomes zero at large pre-strains indicating very little to no strain hardening behavior thereafter. The variation of true tensile strain corresponding to the maximum instantaneous strain hardening exponent, (10^{α}) as a function of compressive pre-straining, ε_o, introduced with prior cold rolling can be represented by the following equation (valid up to pre-strain, ε_o, of 0.41):

$$\text{True strain corresponding to maximum slope} = 35.9 * \varepsilon_o^4 - 33.2 * \varepsilon_o^3 + 11.7 * \varepsilon_o^2 - 1.90 * \varepsilon_o + 0.245 \tag{6}$$

with $R^2 = 0.994$.

The equation for α_s then becomes

$$\alpha_s = \log_{10}\left[35.9 * \varepsilon_o^4 - 33.2 * \varepsilon_o^3 + 11.7 * \varepsilon_o^2 - 1.90 * \varepsilon_o + 0.245\right] \tag{7}$$

Here, β_s is a "Hill factor" derived from the nature of the sigmoidal log–log plots of the true stress–strain curves in Figure 6. The β_s constant as a function of pre-straining can be

represented by the following equation as a function of ε_o, the pre-strain introduced with prior cold rolling and valid up to pre-strain of approximately 0.41:

$$\beta_s = 24.7 * \varepsilon_o^4 - 16.4 * \varepsilon_o^3 + 1.87 * \varepsilon_o^2 + 0.615 * \varepsilon_o + 0.159 \quad (8)$$

with $R^2 = 0.987$

The experimental tensile strain hardening curves, with the compressive pre-strain term considered, could therefore be accurately described by the following sigmoidal equation:

$$\begin{aligned} \log \sigma &= 3.25 + (1.21 * \varepsilon_o + 2.69 - 3.25)\left[1 + \exp(\log \varepsilon - \alpha_s)(\beta_s)^{-1}\right]^{-1} \\ &= 3.25 + (1.21 * \varepsilon_o - 0.554)\left[1 + \exp(\log \varepsilon - \alpha_s)(\beta_s)^{-1}\right]^{-1} \end{aligned} \quad (9)$$

with $R^2 \geq 0.998$.

Here, σ is the true stress in MPa, ε_o is the compressive pre-strain introduced with prior cold rolling. ε is the true tensile strain. α_s is the maximum strain sensitivity which corresponds to the log true strain value where there is a maximum slope of the log–log plot of the true stress–true strain curve. β_s is a "Hill factor" derived from the sigmoidal nature of the log–log plots of the true stress–strain curves. The variable describes the steepness of the sigmoidal curve. The numerical value is given by, $\beta = (3.25 - B)(4 \times n_{ipeak})^{-1}$, where n_{ipeak} is the peak instantaneous tensile strain hardening exponent, which is the maximum instantaneous derivative of the sigmoidal function.

Table II provides a summary of the constants to be used in Eq. [9], as a function of certain values of pct CR.

Table II. Constants α_s, β_s, A, and B in Equation [9] as a Function of Pre-strain in the AISI 301LN Steel

Pre-strain		α_s	β_s	A	B	R^2
Pct CR	ε_o					
0	0	− 0.612	0.157	3.25	2.68	0.999
5	0.05	− 0.751	0.196	3.25	2.74	0.999
14.5	0.16	− 0.905	0.245	3.25	2.88	0.999
19	0.21	− 0.881	0.275	3.25	2.97	0.999
26	0.31	− 0.906	0.265	3.25	3.08	0.999
32	0.38	− 0.835	0.278	3.25	3.13	0.998

*Pct CR is the percentage of prior cold rolling.

Figure 9 shows the calculated vs actual true stress as a function of true strain tensile curves for the pre-strain values below 34 pct prior cold rolling (which is equivalent to compressive true strain of 0.41). The proposed model is therefore shown to be remarkably accurate for pre-strain values below 34 pct prior cold rolling.

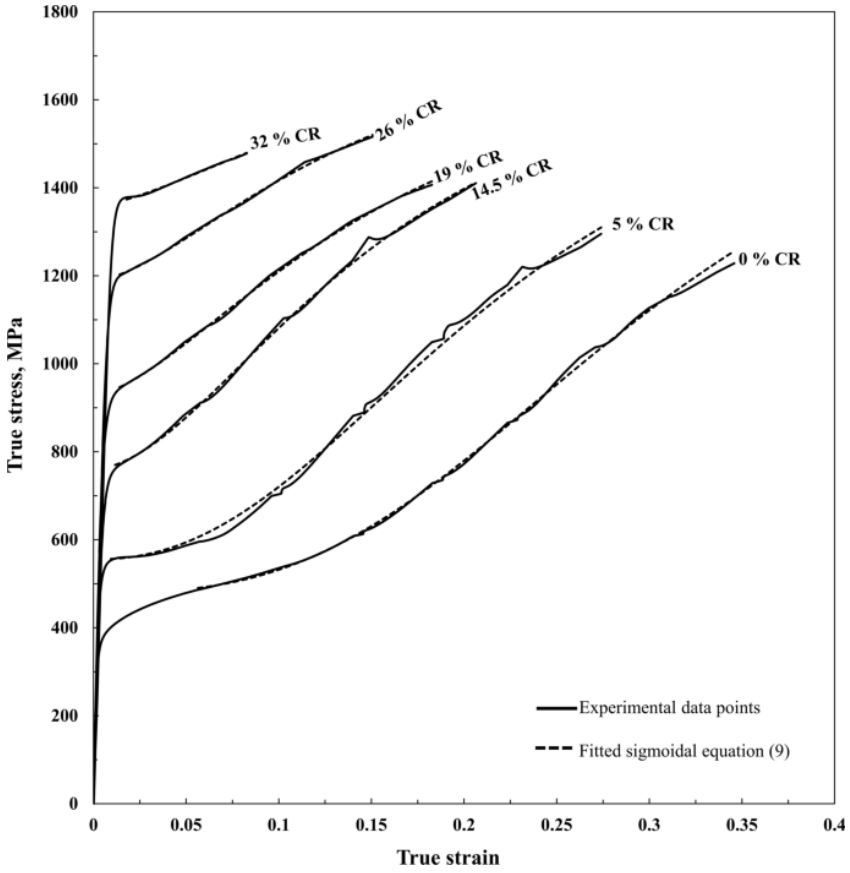

Fig. 9. Calculated vs actual true stress–strain tensile graphs for validation of Eq. [9]

The mechanical energy per unit volume values associated with the tensile strain hardening of prior cold-rolled samples were accurately calculated by numerically integrating the area below the tensile true stress–strain curves (shown in Figure 5, all true stress–strain curves). Figure 10 shows a proportional relationship of the energy absorption of the AISI 301LN as a function of tensile strain applied at 30 °C after various degrees of prior cold rolling, determined using tensile deformation.

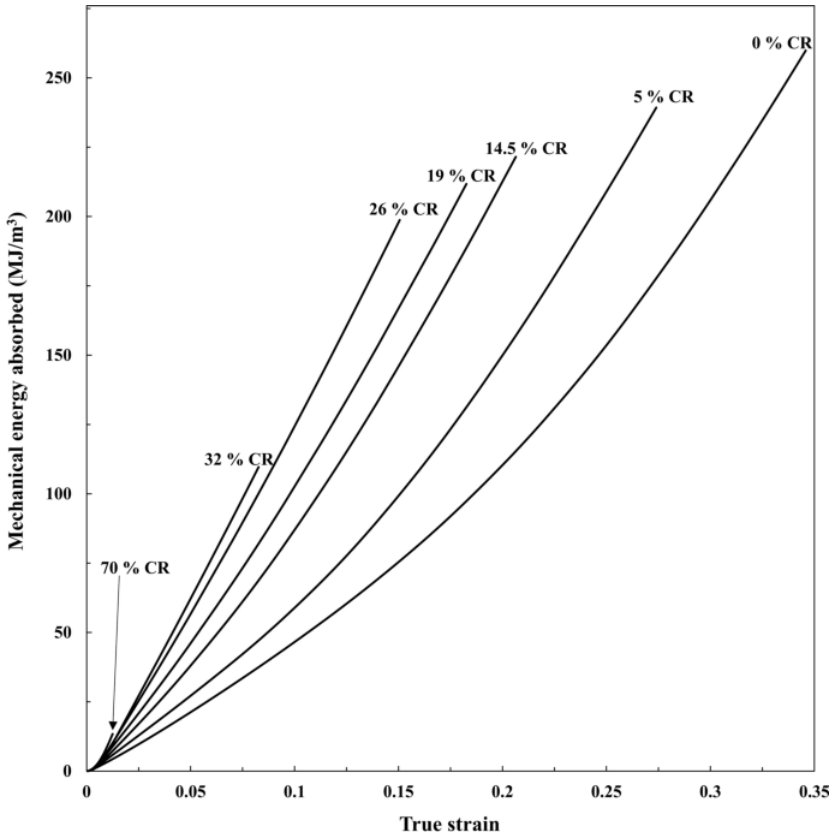

Fig. 10. The mechanical energy absorbed as a function of tensile strain applied to prior cold-rolled samples

As the extent of prior cold rolling increases, the volumetric energy absorbed during uniform plastic deformation decreases to less than 10 MJ/m^3 (at above 70 pct cold rolling) due to significantly impaired uniform tensile strain at high levels of cold rolling. The reduced amount of mechanical energy that can be absorbed by the material after heavily cold deformation makes it inferior in terms of crashworthiness as the material needs to absorb significant amount of energy in the event of a collision. The material with no prior cold rolling absorbs the maximum mechanical energy during tensile deformation, and the performance of the 5 pct CR steel was also good in this regard. As the percentage of prior cold rolling increases, a decrease in mechanical energy that was absorbed by the materials was observed. This decrease in mechanical energy corresponds to the amount of energy absorbed during prior cold rolling as well as the reduced strain hardening ability of the steel (see Figure 7). Therefore, the mechanical energy available for crashworthiness at a given degree of prior cold rolling was calculated as the difference between the mechanical energy absorbed by a material with no prior cold rolling and that after prior cold rolling. Figure 11 shows the maximum cumulative mechanical energy that can be absorbed after a certain degree of prior cold rolling.

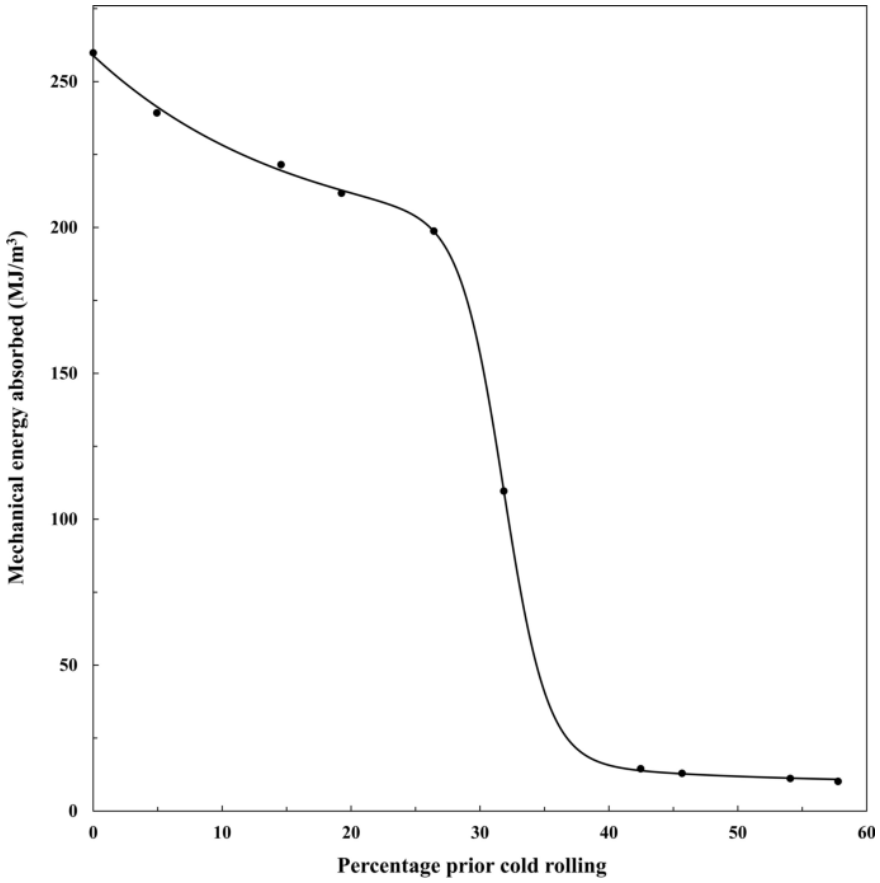

Fig. 11. The mechanical energy available for crashworthiness as a function of percentage of prior cold rolling

There is an abrupt decrease in the total mechanical energy absorption capabilities after 30 pct prior cold rolling as shown in Figure 11 due to abrupt decrease in tensile uniform strain corresponding to 30 pct prior cold rolling (see Figure 5). The very low uniform tensile strain after the high degrees of prior cold rolling, (greater than 30 pct) had resulted in limited amount of energy absorption capability of a material. The minimum amount of energy that the material must be able to absorb if used in the making of crash-relevant structures of a vehicle using the ideal yield strength (750 to 920 MPa), tensile strength (1000 ~ 1150 MPa), and uniform tensile strain of at least 22 pct,[24] has been calculated as being 210 MJ/m^3 (an area under a true tensile stress–strain curve satisfying minimum mechanical requirements). This makes cold rolling of 20 pct, the maximum possible final temper rolling that can be applied to this material. However, other required mechanical properties such as yield strength, tensile strength, hardness, elongation to fracture may limit the range of percentage of final temper rolling that can be applied to this material.

4 Discussion

The lower strain hardening response in tension after prior compressive straining through cold rolling and consequent prior strain-induced α'-martensite formation is shown in Figure 8 and indicates that there is a limit to the useful prior cold rolling that can be employed if good tensile energy absorption is required. This behavior can be accounted for by the following effects of increasing the prior compressive straining; an increase in SFE in the austenite will follow with

increased prior cold rolling as well as a reduction of the austenite volume fraction, which is inherently more strain hardenable.

The work done by Mahato *et al.*,[25] showed a strong increase in SFE with the increase in deformation from steels from 19.9 mJ/m^2 at 2 pct tensile strain, 23.4 mJ/m^2 at 5 pct tensile strain to over 40 mJ/m^2 at 46 pct tensile strain, and austenitic dislocation density deformation of TWIP steels was observed. Their work demonstrated that the SFE value is directly proportional to the dislocation density of the austenite.

In the present work, bulk measurements of austenite, α' martensite, and ε-martensite induced as a function of percentage cold rolling of selected samples, determined using neutron diffraction analyses had shown an increase in the ε-martensite to a maximum around 15 pct cold rolling which then decreases to zero at higher percentage of cold rolling (refer to Figure 1). This has been confirmed by the EBSD analysis which was done on 10 and 30 pct cold-rolled samples, where significant amount of ε-martensite could be observed in a 10 pct cold-rolled sample and no ε-martensite could be easily seen in a 30 pct cold-rolled sample (refer to Figure 3).

The equations developed and described here to model the tensile strain hardening behavior of the metastable austenitic stainless steel studied can be used in the numerical simulation of the energy absorbed by structures during collision events. In addition, it can also be used to establish the maximum prior compressive strain through cold work which will still result in a steel capable of adequate energy absorption during a collision event. From Eq. [9], for the term $(1.21\varepsilon_o - 0.554)$ to be equal to zero, the pre-strain, ε_o should be 0.41 (34 pct prior cold rolling). The sigmoidal equation [9] then reduces to $\log \sigma = 3.25$, and at this high level of cold rolling and strength, little to no strain hardening and energy absorption is found (see Figure 5). This is because the value of the B term would then be equal to the value of A (= 3.25), which corresponds to the martensitic saturation value at 30 °C. Therefore, the sigmoidal equation [9] is only valid up to compressive pre-strain values of ~ 0.41 (34 pct prior cold rolling). It is recommended that some of the tensile flow hardening work be repeated at higher strain rates, in order to include a strain rate term in Eq. [9] in future work.

5 Conclusion

1. For the metastable austenitic AISI 301LN stainless steel studied, a modified Boltzmann sigmoidal model was developed and found to adequately describe the tensile strain hardening behavior of material compressively pre-strained through cold rolling, up to a maximum value of a prior compressive true strain of 0.41. These equations can be used in the numerical simulation of the energy absorbed during collision events of structures from this steel. In addition, it can also be used to establish the maximum prior compressive strain through cold work which will still result in a steel capable of adequate energy absorption.
2. The prior compressive straining and the resultant formation of martensite (both alpha and epsilon) significantly reduce the subsequent strain hardening response in tension, due to an increase of SFE and dislocation density and due to the inherently lower strain hardening response of martensite compared to austenite. At high initial amounts of austenite and relatively low pre-strain values, very high instantaneous tensile strain hardening exponents result. The strain hardening behavior is directly correlated with the ability of the material to absorb mechanical energy during a collision.

3. In order to produce AISI 301LN crash-relevant structures for a vehicle, a cold rolling thickness reduction in the order of 20 pct or lower must be employed. This will result in the mechanical energy absorbed by the material of at least 210 MJ/m^3 in the event of a collision. The tensile strain hardening curves established for the pre-strained steel confirmed a high-strength coefficient with a value in the range of 1770 to 1790 MPa for the AISI 301LN steel at 30 °C and as confirmed by the tensile strength of 1715 MPa, which was obtained after a prior cold rolling of 63.2 pct (true compressive strain of 1.0).

Acknowledgments

The authors are grateful to Columbus Stainless Steel (Pty) Ltd for financial support as well as providing the material, Department of Science and Technology, S.A. Government, through their AMI - FMDN (Advanced Materials Initiative - Ferrous Metals Development Network) programme, administered by Mintek, for financially supporting this work, and NECSA for their neutron diffraction service and assistance. The assistance of Prof Johan de Villiers in the interpretation of neutron diffraction data is gratefully acknowledged.

Competing interest

The authors declare that they have no known competing financial interests or personal relationships that could have appeared to influence the work reported in this paper.

References

1. L.E. Murr, K.P. Staudhammer, and S.S. Hecker: *Metall. Trans. A*, 1982, vol. 13, pp. 627–35.
2. T.W. Mukarati, R.J. Mostert, and C.W. Siyasiya: *IOP Conf. Ser. Mater. Sci. Eng.*, 2019, vol. 655, p. 012008.
3. D.P. Rao Palaparti, B.K. Choudhary, E. Isaac Samuel, V.S. Srinivasan, and M.D. Mathew: *Mater. Sci. Eng. A*, 2012, vol. 538, pp. 110–17.
4. L.P. Karjalainen, T. Taulavuori, M. Sellman, and A. Kyröläinen: *Steel Res. Int.*, 2008, vol. 79, pp. 404–12.
5. S.H. Li, W.J. Dan, W.G. Zhang, and Z.Q. Lin: *Comput. Mater. Sci.*, 2007, vol. 40, pp. 292–99.
6. K.K. Singh: *Mater. Sci. Technol.*, 2004, vol. 20, pp. 1134–42.
7. T.W. Mukarati, R.J. Mostert, and C.W. Siyasiya: *Mater. Sci. Eng. A*, 2020, vol. 792, p. 139741.
8. M. Cohen and G.B. Olson: *Metall. Trans. A*., 1975, vol. 6A, pp. 791–95.
9. H.C. Shin, T.K. Ha, and Y.W. Chang: *Scr. Mater.*, 2001, vol. 45, pp. 823–29.
10. P. Santacreu, J. Glez, G. Chinouilh, and T. Frohlich: *Steel Res. Int.*, 2006, vol. 77, pp. 686–91.
11. N. Tsuchida, Y. Yamaguchi, Y. Morimoto, T. Tonan, Y. Takagi, and R. Ueji: *ISIJ Int.*, 2013, vol. 53, pp. 1881–87.
12. N. Tsuchida, T. Kawahata, E. Ishimaru, and A. Takahashi: *ISIJ Int.*, 2014, vol. 54, pp. 1971–77.
13. P.M. Ahmedabadi, V. Kain, and A. Agrawal: *Mater. Des.*, 2016, vol. 109, pp. 466–75.
14. S.S.M. Tavares, J.M. Pardal, M.J. Gomes, H.F.G. Abreu, and M.R. Silva: *Mater. Charact.*, 2009, vol. 60, pp. 907–11.
15. M. Naghizadeh and H. Mirzadeh: *Vacuum*., 2018, vol. 157, pp. 243–48.

16. F. Peng, X. Dong, K. Liu, and H. Xie: *J. Iron Steel Res. Int.*, 2015, pp. 931–36.
17. T.W. Mukarati, R.J. Mostert, and C.W. Siyasiya: *Steel Res. Int.*, 2021, vol. 2100459, pp. 1–14.
18. A.M. Beese and D. Mohr: in *SEM 2009 Annu. Conf. Expo. Exp. Appl. Mech. Albuquerque New Mex.*, 2009, vol. 2009, pp. 1–7.
19. J. Talonen, P. Aspegren, and H. Hänninen: *Mater. Sci. Technol.*, 2004, vol. 20, pp. 1506–12.
20. T.W. Mukarati, R.J. Mostert, and C.W. Siyasiya: *Mater. Sci. Eng. Conf. Ser.*, 2018, vol. 430, p. 12042.
21. T.W. Mukarati: PhD Thesis, UPSpace, University of Pretoria, 2020.
22. G. Dini, A. Najafizadeh, R. Ueji, and S.M. Monir-vaghefi: *Mater. Des.*, 2010, vol. 31, pp. 3395–402.
23. G.C. Soares, M.R.M. Carla, and L. De Arruda Santos: *Mater. Res.*, 2017, vol. 20, pp. 141–51.
24. S. Srikanth, P. Saravanan, V. Kumar, D. Saravanan, L. Sivakumar, S. Sisodia, and K. Ravi: *Int. J. Metall. Eng.*, 2013, vol. 2, pp. 203–13.
25. B. Mahato, S.K. Shee, T. Sahu, S. Ghosh Chowdhury, P. Sahu, D.A. Porter, and L.P. Karjalainen: *Acta Mater.*, 2015, vol. 86, pp. 69–79.